Advances in Applied Energy 18 (2025) 100218

Contents lists available at ScienceDirect

Advances in Applied Energy

journal homepage: www.elsevier.com/locate/adapen

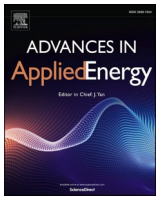

Investigation of a novel separately-configured thermoelectric cooler: A pathway toward the building integrated thermoelectric air conditioning

Haowen Liu [a,d], Limei Shen [b], Yunhai Li [a], Xudong Zhao [a,*], Guiqiang Li [c], Zeyu Liu [b], Hongxing Yang [d]

[a] Centre for Sustainable Energy Technologies, University of Hull, HU6 7RX, UK
[b] School of Energy and Power Engineering, Huazhong University of Science and Technology, 430074, PR China
[c] Department of Thermal Science and Energy Engineering, University of Science and Technology of China, Hefei, 230027, PR China
[d] Department of Building Environment and Energy Engineering, The Hong Kong Polytechnic University, Hong Kong, PR China

ARTICLE INFO

Keywords:
Thermoelectric cooler
Separately-configured
Bridge for internal phonon and electron transfer processes

ABSTRACT

Due to structural limitations, the hot and cold sides of conventional thermoelectric coolers (TECs) are fully integrated, making it challenging to directly incorporate TECs into building facades or ceilings to utilize natural ventilation from the building exterior assisting cooling the hot junction. This constraint renders TECs unsuitable for direct application in building façade. To overcome these challenges, an innovative separately-configured thermoelectric cooler (SC-TEC) has been developed. This original design enables the direct integration of TECs into building façades for air conditioning while utilizing the outdoor environment as auxiliary cooling for the TEC's hot side, thereby enhancing overall system performance. Our preliminary study showed that, in a TECs-ceiling system, the novel SC-TEC achieves a 13 % higher cooling capacity compared to a traditional TEC-ceiling. The unit cooling output increased from 16.66 W/m^2 to 18.82 W/m^2. And the temperature profiles shows that the cooling capacity of the SC-TEC could be further enhanced with a higher-performance connecting material. Given its advantages, such as no moving parts, noiseless operation, and efficient heat transfer, the SC-TEC has potential to open up new research direction in the building-TEC sector.

1. Introduction

With the enormous building construction in advanced and emerging economies, the energy demand and carbon emissions from building continues to rise. In 2023, the buildings and construction sectors together account for 30 % of global energy consumption and 27 % of carbon emissions [1]. To align with the net zero scenario, carbon footprints from buildings need to be reduced by more than two-thirds by 2030, which requires significant efforts on clean and efficient technologies in all end-uses [1,2]. In modern buildings, air-conditioning system is the major energy consuming part responsible for 30 % of the buildings' energy consumption and 40 % of the landlord consumption [3]. To-date, most air conditioning systems adopt vapor compression refrigeration cooling technology which has high level of electrical energy consumption and enormous carbon emissions, and creates severe health hazards owing to the use of environment-unfriendly refrigerants.

Thermoelectric modules (TEMs), as an emerging technology, present a potential alternative to conventional mechanical vapor compression systems, with the virtues of high reliability, noise-free, solid-state structure, and free of fluid/gas [4]. Thermoelectric coolers generate a temperature gradient in the semiconductor elements when an electric current is applied. The performance of a TEC is typically measured using the Coefficient of Performance (COP), which is defined as the ratio of the cooling capacity Q_c to the power consumed W.

Currently, widely used commercial TECs achieve a coefficient of performance (COP) exceeding 3.5 at low temperature differences (Fig. 1a). Moreover, state-of-the-art thermoelectric materials have been shown to achieve a COP exceeding 8 under laboratory conditions (Fig. 1b) [5]. These advancements highlight the promising potential of TECs as alternative air conditioning solutions for buildings.

To date, the building integrated thermoelectric cooling technology has gained noteworthy attention due to its effective and environmental-friendly characteristics. Some preliminary research on the TEC-building integrated system have been conducted. Riffat et al. reported a TEC assembly (eight modules) designed for small-scale space air conditioning applications in buildings. This device demonstrated up to 220 W of

* Corresponding author.
E-mail address: Xudong.zhao@hull.ac.uk (X. Zhao).

https://doi.org/10.1016/j.adapen.2025.100218
Received 7 December 2024; Received in revised form 3 March 2025; Accepted 8 March 2025
Available online 9 March 2025

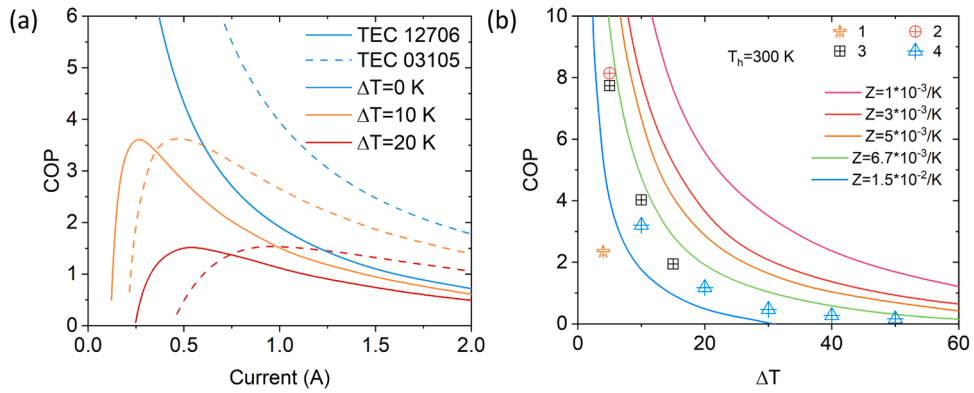

Fig. 1. (a) The COP of different commercial thermoelectric coolers with varying current and temperature difference. The lines at $\Delta T = 10$ K and 20 K represent the test values for two commercial TECs provided by the manufacturer, while the lines at $\Delta T = 0$ K corresponds to the theoretical COP limits. (b) the COP versus temperature difference [4]. The symbols represent experimental values from the following modules: (1) A 7-pair n-$Mg_{3.2}Bi_{1.4975}Sb_{0.5}Te_{0.0025}$/p-$Sb_{1.5}Bi_{0.5}Te_{2.91}Se_{0.09}$ module, (2) A commercial Bi_2Te_3-based module, (3) An n-$Mg_3Bi_{1.5}Sb_{0.5}$/p-α-MgAgSb module, and (4) A commercial UT15–200-F2–4040 module. The solid lines are calculated at Th = 300 K using several typical Z values.

cooling capacity with COP of 0.46, which means TECs can meet the cooling requirement for small-scale buildings [5]. Substantial works on TEC-based cooling systems have been conducted, exploring various integration patterns and optimization approaches, to address performance limitation. Thermoelectric air ducting system involves the integration of TEC modules within the air ducts (TE-AD) to provide cooling in buildings [6]. In 2015, Irshad investigated the dehumidification process of air in TE-AD system, which could reduce building space temperature by 1.2 °C to 5.3 °C, coupled with 5 % to 31 % indoor relative humidity changes [7]. With the combination of the PV wall and

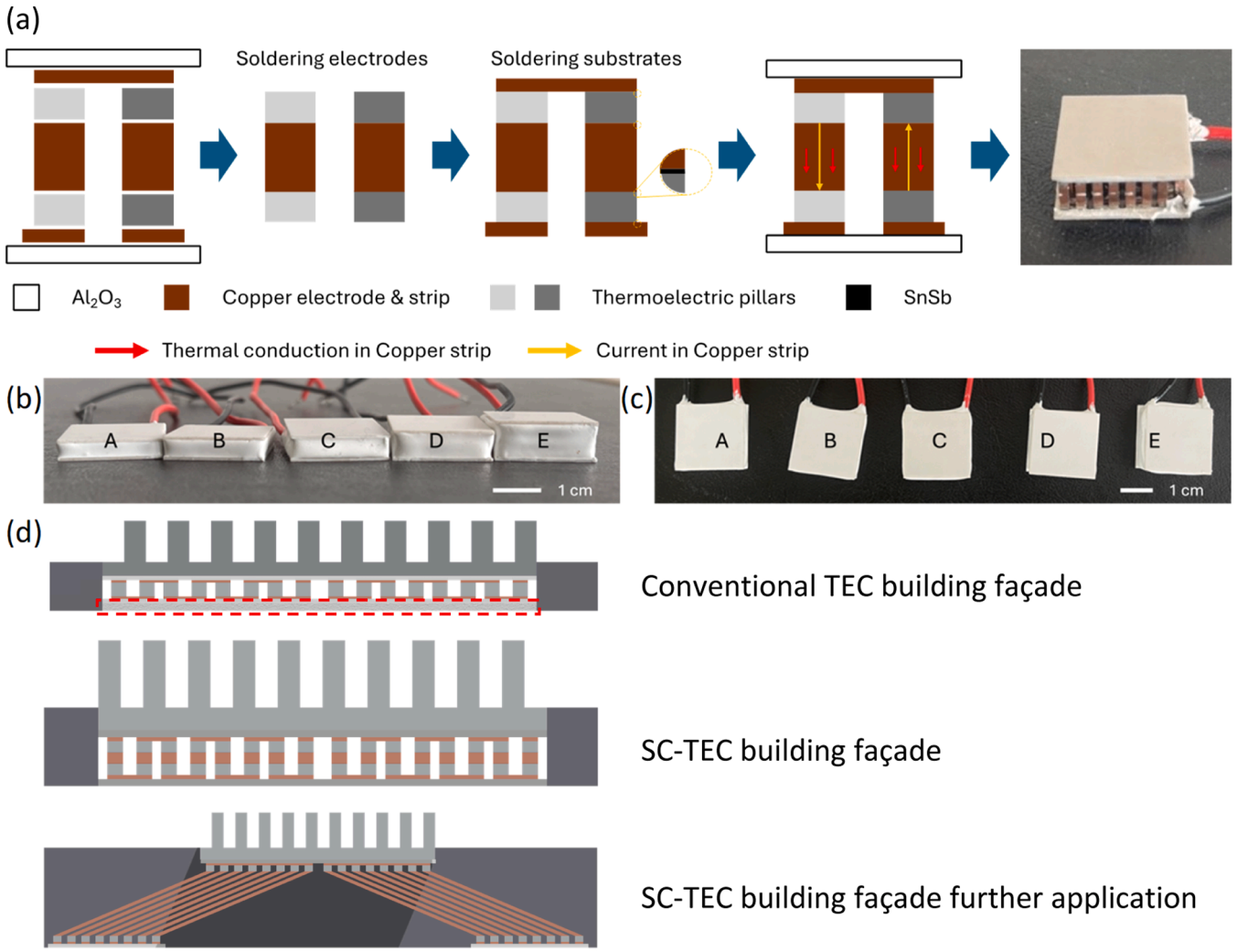

Fig. 2. Fabrication process and potential applications of the SC-TEC.

TE-AD system, the COP of TE cooling increases from 0.679 to 1.15 [8]. Irshad further explored the economic study of the TE-AD system. Compared with the existing air conditioning system, the TE-AD system achieved economic saving of US$ 127.34/year and additional benefits of Freon free [9,10]. Allouhi used TRNSYS to predict the thermal behavior of a TE-heating system coupled with office space [11]. Kim presents a mathematical model for TE-AD system based on three different cases and investigated optimal performance [12]. Cai designed a TE-AD heat recovery unit that utilized the thermoelectric refrigeration process to actively recover waste heat from the air exhausted from buildings. The operational cost of the TE-AD heat recovery system could be as low as 0.024 $/kWh and could be further reduced with an increase in the figure of merit (ZT) [13,14]. Considering heat conduction, the TE-AD system with parallel/counter flow arrangement of hot and cold junction is expected to have different energy performance [15,16]. Previous studies indicated that the counter flow arrangement could achieve a lower temperature difference between hot and cold fluids compared with parallel arrangement [17]. Thus, the TE-AD system has been subject to extensive theoretical and experimental investigation.

Except for the TECs air ducting systems, some researchers have explored integrating thermoelectric modules with photovoltaic (PV) or photothermal (PT) systems as auxiliary devices for zero-carbon buildings [18–22].However, one of the main limitations hindering its development is the requirement to integrate the TE components into air ducts, or outdoor equipment, which occupies the additional building space.

The building envelope plays a vital role not only in the thermal comfort but also in building energy efficiency. Incorporating thermoelectric cooler into the building envelope presents significant opportunities for addressing the aforementioned challenges [23]. Two fundamental integration formats are the TE wall [24–29] and the TE radiant panel ceiling [30–33]. These two approaches regulate the indoor environment of buildings by integrating Thermoelectric Cooling (TEC) into walls or ceilings. Liu et al. developed an Active Solar Thermoelectric Radiant Wall (ASTRW) system that utilizes solar energy and thermoelectric modules to control heat flow through building walls, reducing thermal loads and providing space heating. Experimental results demonstrate that the system achieves a COP of up to 2.3 and 34.2 % thermal efficiency when powered by a PV system on sunny winter days, with an optimized operation strategy proposed for enhanced performance [24]. The thermoelectric wall systems could be further utilized to control sustainable indoor climate, the key factor for the system include electrical current and air velocity on heat transfer [28]. Given the natural tendency of cool air to sink, thermoelectric radiant ceilings are particularly well-suited for cooling applications. Su introduced an innovative TEC-Radiative sky cooling building envelope to minimize heat gain and deliver space cooling. Optimized designs achieved cooling capacities of 25.49–35.05 W/m^2 and COPs of 2.00–3.01, highlighting its strong potential for applications in hot climates [30].

The prototype of TE-building-envelope can be categorized based on various factors such as heat sinks [34–38], installation positions [39], cooling types (air [34,40]/water [41]/heat pipe [42,43]). These configurations have been extensively studied for their potential in space heating and cooling applications.

TECs are known for their compact structure, with the cold and hot ends being fully integrated. In typical commercial TECs, the distance between the cold and hot ends is generally no >1 cm, which is significantly smaller than the thickness of most building facades. Moreover, the positions of the cold and hot ends are fixed and aligned. This compact design makes it difficult for TECs to be directly embedded into building facades for use. To the best of our knowledge, as the aforementioned challenge, none of the existing approaches address the aforementioned challenge of embedding TECs into building facades while utilizing natural ventilation from the building exterior to assist in cooling the hot junction, thereby reducing energy consumption.

To tackle the above noted challenges, we pioneered an innovative separately-configured TEC (SC-TEC) configuration, which features the middle strip structure as the 'bridge' for the internal transfer process of both phonons and electrons, and enable the separated position of the hot side and cold side of the TEC. By using soldering method, a new material set is formed by sandwiching a middle strip between semiconductor materials, as shown in Fig. 2a. This configuration ensures both electrical and thermal conductivity while flexibly extending the distance between the hot and cold ends. Based on this novel design, four SC-TEC prototypes with different material lengths and one control module were manufactured. The sizes of the SC-TEC prototypes are 20 mm × 20 mm with thicknesses of 4 mm, 4.5 mm, 5 mm, 6 mm, and 8 mm, corresponding to copper leg heights of 0 mm, 0.5 mm, 1 mm, 2 mm, and 4 mm, respectively, and labelled as devices A to E (Fig. 2b and c). Each prototype contains 31 pairs of semiconductor units set (bismuth telluride, Bi_2Te_3 and copper strips) arranged in an 8 × 8 configuration, along with copper connectors, 95Sn-5Sb alloy, and 96 % alumina ceramic (Al_2O_3).

This new TEC structure will be extensively studied in this paper, and the research outcomes will help with the change in future design of TEC as an air conditioning system in buildings. As shown in Fig. 2d, when a traditional TEC is used as a building façade, its size and structural limitations require an additional thermal conduction layer for integration. In contrast, the innovative SC-TEC can be tailored to fit the building structure directly, seamlessly adapting to the façade. Furthermore, thanks to the flexibility of the intermediate copper structure, the SC-TEC allows for the cold and hot sides of the system to be staggered or offset from each other, significantly enhancing its adaptability and application flexibility. Its flexibility in design and installation allows the cold side of the TEC fixed to the internal space of the building for heat absorption and room cooling and the hot side of the TEC fixed to the external space of the building for heat dissipation and dumpling.

The new SC-TEC structure facilitates the integration of its structure with various building elements such as façades, walls, windows, and ceilings, thereby broadening the real-world applications of the TECs for building air conditioning. This enables the improved cooling performance and expanded practicality in areas ranging from building structures to electronics and automotive systems, and thus position the SC-TEC as versatile and promising solution for efficient split air conditioning for buildings and other thermal management needs.

In summary, a novel SC-TEC have been proposed and investigated, this initiative will overcome the restriction of the building fabric on TEC cold- and hot- side connection, enabling the simultaneous heat dissipation to ambient and heat absorption from interior effectively. Compared to traditional TEC systems, the novel design can utilize natural outdoor ventilation as a potential auxiliary cooling mechanism for the hot side, thereby reducing energy consumption. This innovation will radically change the landscape of TEC cooling sector and help transform the TEC cooling into a net-zero and sustainable development track.

2. Research methodology

After the fabrication of the SC-TEC, preliminary testing and simulations are conducted to determine the material correction coefficients. The corrected model is then validated by comparing with experimental results and reference data. Based on the validated model, key performance indicators such as maximum temperature difference, COP, temperature distribution, and the impact of contact resistance are analyzed. Finally, a case study is carried out to evaluate the practical application of SC-TEC in real-world scenarios.

2.1. Prototype fabrication

The separately-configured thermoelectric cooler is manufactured by SAGREON Ltd, based on the commercial model TEC-03,105. A traditional TEC is composed of ceramic plates, metal strips and pairs of P-N junctions consisting of two distinct semiconductor elements. Furthermore, there are thin solder layers as the metal strips and semiconductor

elements are boned together. For SC-TEC, the metal connector is humbly added in the semiconductor elements, while maintaining the original TEC structure. This allows the separation between hot/cold ends to be significantly increased while retaining the original amount of semiconductor consumables.

To facilitate the subsequent analysis of the internal electrical resistance and thermal resistance of the TEC, the internal structure of the TEC will be further elaborated in Appendix A.

2.2. Mathematical model

The Finite element analysis model was adopted to analyze the spatial temperature distribution and heat transfer process. Generally, the mathematical model for TEC can be simplified to one-dimension as its temperature distribution characteristic. To enable the simulation, some simplifications and assumptions have been adopted:

- All thermal/electrical processes within TEC module reach steady state.
- The heat loss by convection and radiation is neglected.
- The thermal/electrical contact resistance at all interfaces are considered due to the increased number of contact surfaces.
- Thermal physical properties of all materials are related to its operational temperature.
- The hot surface temperature is kept constant of 300.15 K.

There are two critical indexes for evaluating the performance of TEC, namely maximum temperature difference and coefficient of performance (COP).

The COP is defined as the ratio between cooling capacity (Q_c) and power comsuption (P). In a p-n pair of TEC, the Q_c, P, and COP can be calculated as:

$$Q_c = (\alpha_p - \alpha_n) I T_c - \frac{1}{2} I^2 R - k(T_h - T_c) \tag{1}$$

$$P = I^2 R + I(\alpha_p - \alpha_n)(T_h - T_c) \tag{2}$$

$$COP = \frac{Q_c}{P} = \frac{(\alpha_p - \alpha_n) I T_c - \frac{1}{2} I^2 R - k(T_h - T_c)}{I^2 R + I(\alpha_p - \alpha_n)(T_h - T_c)} \tag{3}$$

TEC typically incorporate both p-type and n-type materials to achieve a larger temperature difference. In a p-n pair of TEC, based on Eq. (1) the temperature difference can be deducted as:

$$\Delta T = T_h - T_c = \frac{(\alpha_p - \alpha_n) I T_c - \frac{1}{2} I^2 R - Q_c}{k} \tag{4}$$

To establish the coordinate system for the TEC module, the model sets the cold surface as the reference plane and designates the direction perpendicular to the reference plane as the x-axis. The thermal behavior, temperature gradients and other thermal properties in the x-direction relative to the cold surface of the TEC module could be analyzed based on the standardized frame of reference. The detailed process of model construction is provided in the Appendix B.

2.3. Experimental observations

A pilot experiment was conducted to confirm the modified coefficient of thermos-physical properties. Once the modified coefficients were established, an experiment was further conducted to validate the refine model, a comparative analysis was performed between the conventional TEC-03105 and the TEC-03105 with separated-configuration based on the validated model and experimental results. The test platform and testing procedure for the pilot experiment and validated experiment is detailed in Appendix C.

Table 1
The calculated Seebeck coefficient, thermal conductance, and electrical resistivity for entire TEC.

	Experimental value	Simulate value	Modified coefficient =Experimental value/ simulate value
Seebeck coefficient (V/K)	0.012495	0.012783	0.9775
Thermal conductance (W/K)	0.16744	0.10741	1.5589
Electrical resistivity(Ω)	0.67104	0.65855	0.9814

2.4. Parameters adjustment

The COMSOL Multiphysics software was adopted to solve the finite element model and the simulation results were validated with previous reference and experiment results. For the Multiphysics model of separately-configured thermoelectric module, the relative thermos-physical properties in this research includes the temperature-dependent Seebeck coefficient, thermal conductivity, and electrical resistivity of the chosen thermoelectric material, such as Bismuth Telluride. Also, for copper and 95Sn-5Sb solder, it is necessary to know their thermal conductivity and electrical resistivity, for alumina ceramic, it is important to know its thermal conductivity since they are not involved in the circuit. These properties are obtained from marital library in COMSOL Metaphysical software and are known to vary with temperature.

However, in practical application and experimental testing scenarios, relevant parameters undergo alterations. Therefore, it becomes necessary to introduce modified coefficients to adjust the material parameters. By comparing the experimental values calculated from test data with the simulated values based on theoretical parameters, the modified coefficients for the main thermos-physical properties can be obtained and shown in Table 1. The detailed calculation process of the modified coefficients is presented in Appendix D.

2.5. Simulation model validation

Utilizing an appropriate grid has been demonstrated to be beneficial in improving the precision and effectiveness of the model computations. After completing the meshing process, the model requires further validation. By presenting a side-by-side comparison of cooling capacity and coefficient of performance value with pervious reference data, a commendable level of congruence emerges between the simulation results and the corresponding data from established references. The noteworthy aspect here is the minimal deviation observed. Specifically, the maximum relative errors in cooling capacity and coefficient of performance are confined to 4.88 % and 3.51 %, respectively.

The model has been further validation with experimental results. For the FIVE types of the new SC-TEC prototypes (included 1 control module), the experiment-simulation discrepancies in hot-cold surface temperature difference are within 2 K which can be attributed to margin of error in the testing process. This level of alignment signifies that the simulation model has been adeptly calibrated and accurately captures the underlying physical phenomena, bolstering the confidence in its predictive capabilities. This outcome further strengthens the foundation for subsequent analyses and findings derived from the simulation, affirming the credibility of the insights gained through this research.

The detailed mesh generation and convergence verification are presented in Appendix E.

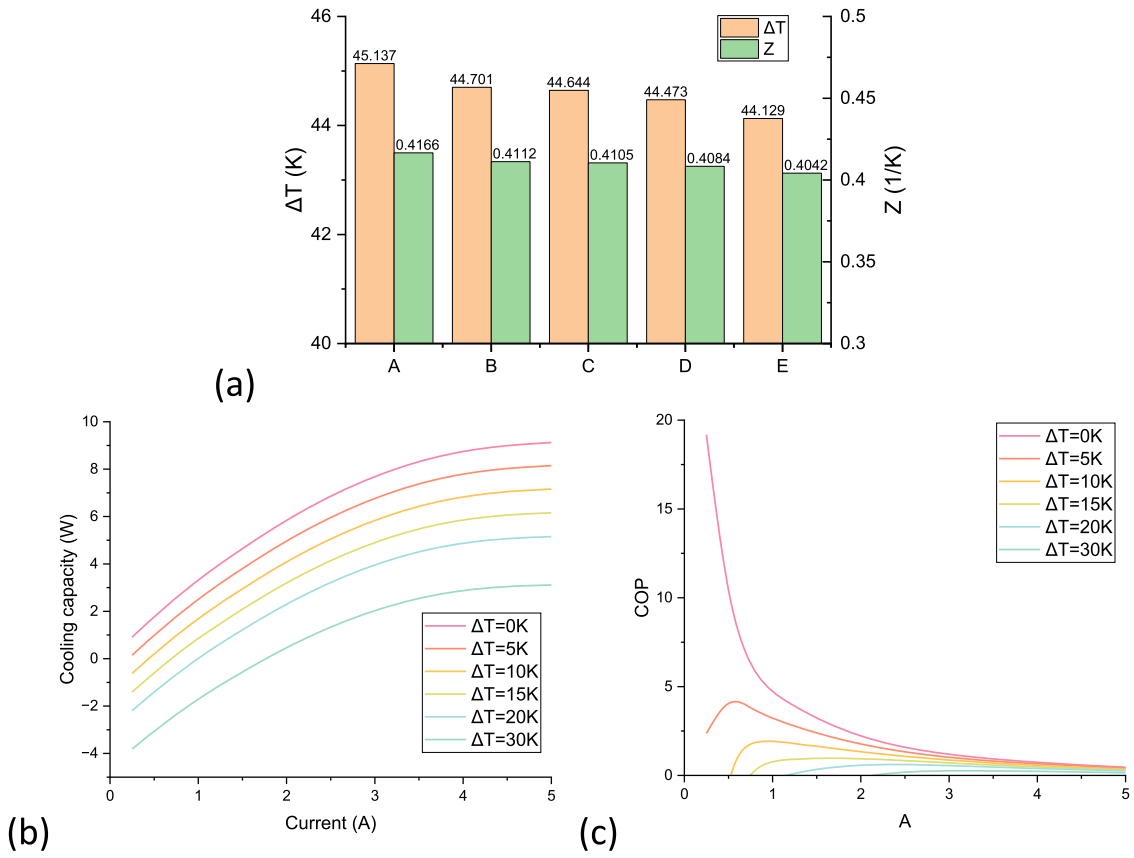

Fig. 3. Main evaluation indexes (a) Maximum temperature difference and figure of merit Z for devices A-E; (b) Cooling capacity variation with current and ΔT; (c) Coefficient of performance varying with current and ΔT.

3. Results and discussion

3.1. Characterization of SC-TEC prototypes

We use the experimental setup described in Section 2.3 to evaluate the performance of SC-TEC prototypes, and the theoretical and simulation models were validated against the test results presented in Section 2.5. The characterization analysis could be further expanded based on the validated model, offering deeper insights into device behavior.

Generally, the main evaluation indicators of TEC include the maximum temperature difference, cooling capacity, and COP.

The maximum temperature difference for each device is shown in Fig. 3a. Obviously, the maximum temperature difference for these prototypes can exceed 40 K. For the SC-TECs, the maximum temperature difference shows a slight attenuation compared to the control module, with approximately 1 K of attenuation when the device height is doubled. This reduction is primarily due to the adverse impact of Joule heat generated by the metal strips. As the length of the metal strips increases, the amount of Joule heat also rises, leading to a decrease in the maximum temperature difference. However, since metal has low electrical resistance, the magnitude of this effect remains relatively small. Additionally, the Figure of Merit (Z), calculated using the Eq. (2)$\Delta T_{max}/(T_h - \Delta T_{max})^2$ [44], follows a similar trend due to the same influencing factors.

To further analyze the performance of the SC-TEC, we conducted simulations of cooling capacity and coefficient of performance under various operational conditions with temperature differences of 5 K, 10 K, 20 K, and 30 K. Extremely operational conditions are not typically encountered in residential buildings, so operational conditions with ΔT greater than 30 K are not considered in our analysis.

For TECs, cooling capacity is closely related to the cooling demand, while COP reflect to efficiency. Fig. 3b and c illustrate the variations in cooling capacity and COP with current and temperature difference, respectively.

As can been seen in Fig. 3b, the cooling capacity is simultaneously affected by both ΔT and the current. Apparently, the cooling capacity continuously declines as the temperature difference between the hot and cold surfaces increases. This can be explained by the fact that a portion of the cold is consumed to maintain the temperature difference.

Further, with the current increasing, the cooling capacity increase progressively, but the increase rate gradually diminishes. In fact, the cooling capacity includes both the cold generated by Seebeck effect and the heat generated by Joule heating. Under small currents, the Seebeck effect dominates, as the current increase, the increment of Joule heating surpasses the increments of Seebeck cooling, which leads to a flattening of cooling capacity curve. As the current further increases, Joule heating becomes dominant, resulting in a continuous decrease in cooling capacity until its failure.

Fig. 3c shows the tendency of COP varying with current at different ΔT. As the current increases, the COP initially rises, reaches a peak, and then gradually declines. As previously discussed, the cooling capacity is influenced by both the Seebeck effect and Joule heating. At low currents, the impact of Joule heating on COP is relatively small. During this stage, the rapid increase in cooling capacity leads to a sharp rise in COP. However, as the current continues to increase, the growth rate of cooling capacity slows down while power consumption gradually rises. Consequently, the ratio of these two factors, i.e., the COP, begins to decline. Meanwhile, as the temperature difference between the hot and cold sides increases, the peak COP gradually decreases, while the corresponding optimal current steadily shifts to higher values.

Based on Fig. 3b and c, both the cooling capacity and COP of the TEC decrease as the temperature difference increases. For TECs integrated

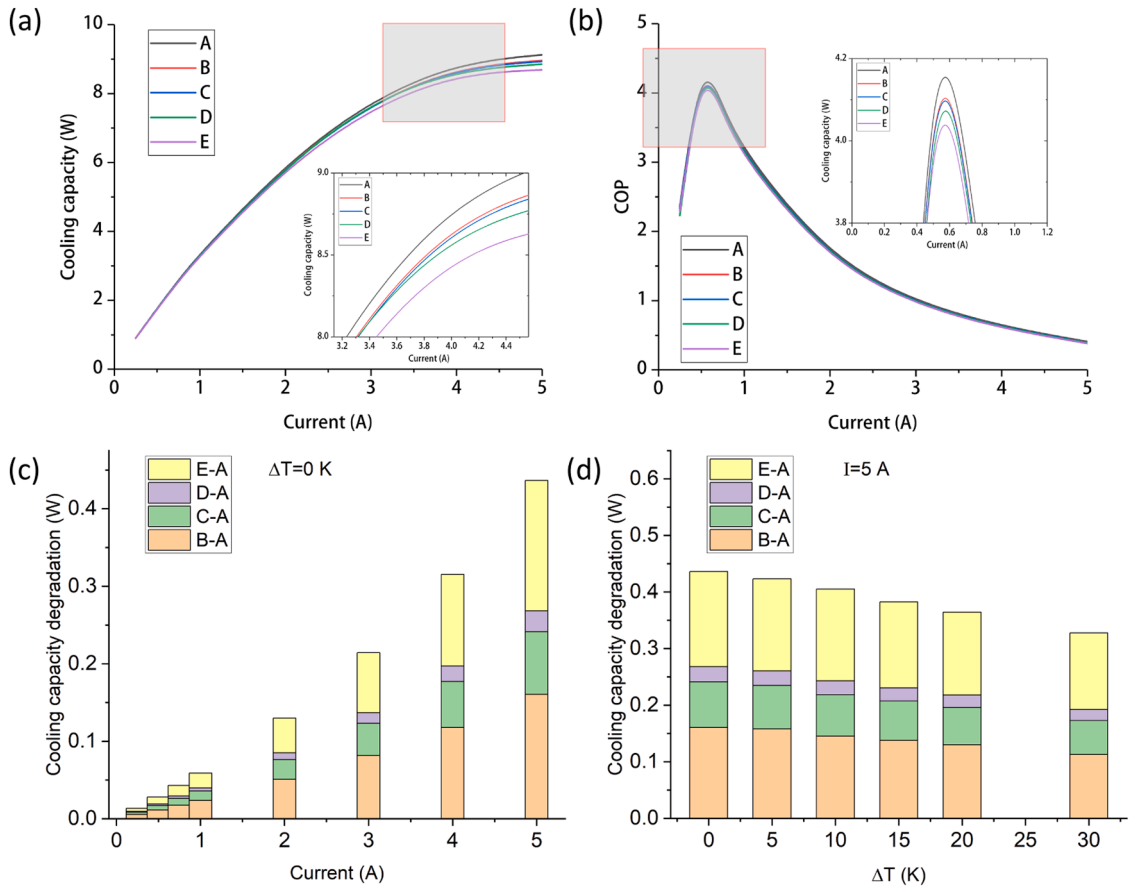

Fig. 4. Performance analysis of devices A–E under varying current and temperature difference (a) Cooling capacity variation with current at ΔT=0 K; (b) COP variation with current at ΔT=5 K; Performance decrement variation (c) with current at ΔT=0 K; (d) with ΔT at $I = 5$ A.

with buildings, the temperature difference between the hot and cold sides is typically not large. For instance, at a temperature difference of 10 K, the cooling capacity can reach 7.13 W, and the maximum COP is 1.93.Regarding current variation, high cooling capacity occurs in the higher current range (over 4 A), while the optimal COP is observed in the lower current range (<3 A). For building applications, it is essential to balance cooling capacity and COP to determine the appropriate operating current for TEC systems. It is noteworthy that TEC/SC-TEC exhibits excellent cooling power density. The cooling capacity per unit area could exceed 15 kW/m^2 under a high current ($I = 5$A), even at a low current ($I = 0.5$A). The limit of the cooling capacity of SE-TEC is 500 W/m^2.

Fig. 4a and b illustrate the variation of cooling capacity for device A-E at a temperature difference of 0 K and variation of the COP at a temperature difference of 5 K, respectively. For the SC-TEC, the trends in both cooling capacity and COP with respect to temperature and current follow a similar pattern to the performance trends discussed earlier for TECs. Additionally, as the length of the middle strip increases, both the cooling capacity and COP slightly decrease. This performance degradation is primarily due to the Joule heating generated by the middle strip and the contact effects introduced by the additional interfaces. However, the overall impact on performance is relatively small. When the height of the entire TEC is doubled (device E), the reduction in both cooling capacity and COP is <5 %.

As shown in Fig. 4c and d, the decrement for SC-TEC's cooling capacity increases gradually with increasing current and decreases with increasing temperature difference. This is because, as the current increases, the additional Joule heating generated by the metal strips increases, leading to a higher degradation value. On the other hand, when the temperature difference increases, the resistivity of the metal strips slightly decreases, reducing the additional Joule heat, which results in a smaller degradation value. Further analysis reveals that the increase in the height of the SC-TEC metal strip does not have a linear relationship with the cooling capacity decrement. This is due to the presence of contact thermal resistance and contact electrical resistance. When the metal strip height is small, contact effects dominate. As the height increases, Joule heating gradually becomes the primary factor affecting performance. Therefore, in the future practical application of SC-TEC, it would be beneficial to consider the ratio between the TE material and the metal strip to optimize the design.

3.2. *Performance of TECs with separated-configuration with different hot-end temperature scenarios*

The previously mentioned sections analyzed the variations in cooling capacity and COP of TECs with separated configuration structure as a function of operating current under the condition of a hot-side temperature of 27°C, i.e., 300.15 K. However, in practical scenarios, environmental temperatures in their natural states often exceed 30°C. Therefore, in this section, an analysis of the performance of TECs with a separated configured structure is conducted under hot-side temperatures of 30°C, 35°C, and 40°C. This further examines the influence of temperature variations on TEC performance and how the separated configured structure affects TEC performance as temperature changes.

For device A, the trends of cooling capacity and COP with varying current at different hot-side temperatures under temperature difference of 0 K are depicted in Fig. 5a and b. With the increase in hot-side temperature, both cooling capacity and energy consumption show an upward trend. This is a result of the material's response to temperature changes. Around 300 K, the Seebeck coefficient and electrical resistivity

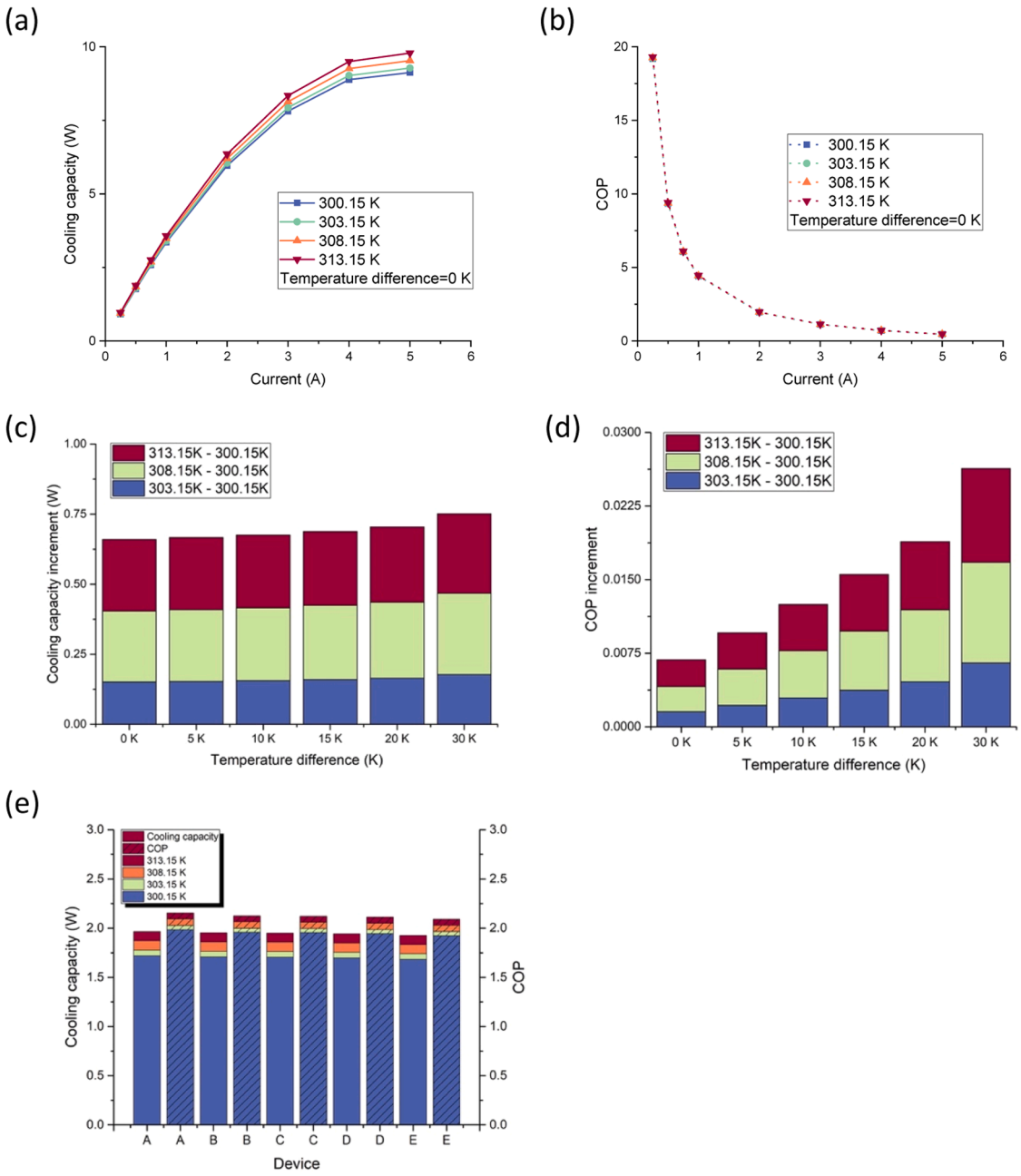

Fig. 5. Effects of hot-side temperature and current on the performance, the trend of (a) cooling capacity; (b) COP with varying current at different hot-side temperatures for device A under temperature difference of 0 K; The trend of (c) cooling capacity increments, (d) COP increments with variations in the hot-side temperature compared to the reference temperature of 300.15 K, for hot-side temperatures of 303.15 K, 308.15 K, and 313.15 K under current of 5 A; (e) The variations in cooling capacity and COP with an increase in hot-side temperature for different TECs with separated configuration structures under current of 1 A, temperature difference of 10 K.

of Bismuth Telluride materials increase with temperature, leading to an increase in cooling capacity and energy consumption. However, overall, the increase in cooling power is more significant, resulting in a slight improvement in the COP.

Fig. 5c and d illustrate the trends in the increments of cooling capacity and COP as the hot-side temperature varies relative to the reference temperature of 300.15 K, for hot-side temperatures of 303.15 K, 308.15 K, and 313.15 K under a current of 5 A. As the hot-side temperature increases, both the cooling capacity and COP increments show an upward trend. Additionally, with an increase in the temperature difference between the hot and cold ends, the increments in cooling capacity and COP also gradually increase. This phenomenon is closely related to the behavior of Bismuth Telluride, specifically its Seebeck coefficient and electrical resistivity, as they vary with temperature.

In Fig. 5e, the variations in cooling capacity and COP with an increase in hot-side temperature are shown for different TECs with separated configuration structures. For all five devices, both cooling capacity and COP increase as the hot-side temperature rises. Furthermore, with an increase in the length of the middle copper connector in the separated configuration structure, the increments in cooling capacity and COP resulting from the increase in hot-side temperature slightly decrease, although the reduction is not very significant.

3.3. *Temperature profile of the SC-TEC prototypes*

By analyzing the temperature profile of the SC-TEC, we can gain a

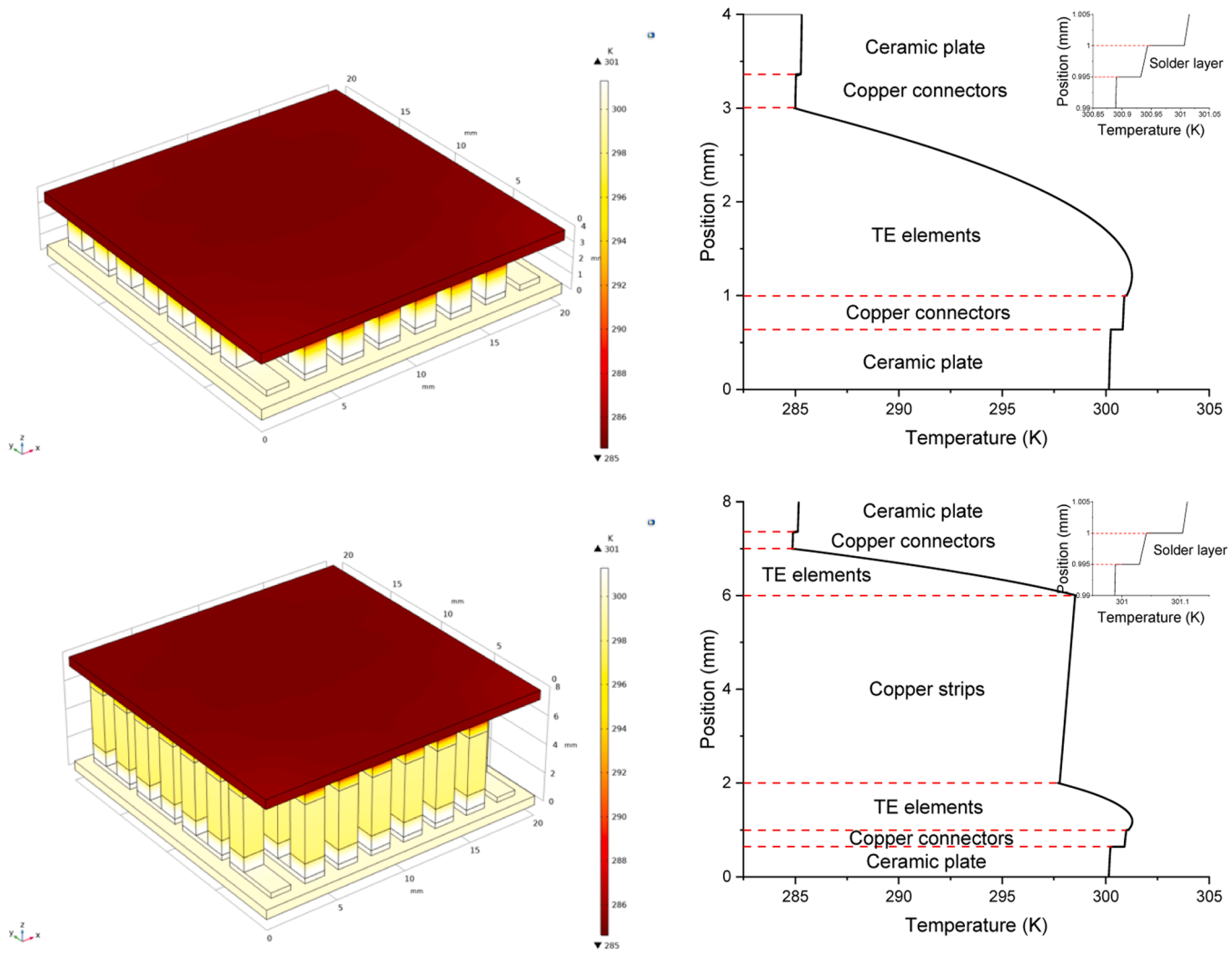

Fig. 6. Temperature distribution for the devices A and E.

deeper understanding of the impact of the metal strip on the overall temperature distribution of the TEC. Fig. 6 depicted the temperature distribution for devices A and E, when the ΔT is 15 K and current is 3 A. Due to the Fourier heat conduction within the ceramic plate, there is a slight increase in the internal temperature. In the copper connector, there is a similar temperature distribution, nonetheless, it is caused by both Fourier heat and Joule heat. In the TE elements, apart the former two effects, there is also the Seebeck effect, which causes the temperature to gradually decrease from the slightly elevated hot surface to the cold surface. For each contact surface, there is a temperature step due to the contact thermal resistance.

Compared to device A, device E with copper strips occurs a temperature increase in the copper strips. The additional heat is generated by the Joule effect of copper strips. Eventually, for the SC-TEC, copper strips serve as a "bridge" for the internal transfer process of both phonons and electrons. A future material with low thermal and electrical resistance could eliminate this negative effect, enabling the achievement of lossless performance in the SC-TEC.

Based on the above experimental and simulation results, as well as associated analysis, it can be inferred that the SC-TEC may exhibit a slight performance loss compared to traditional TECs, the overall performance degradation is not significant. But, for SC-TEC integrated with building systems, the hot side of the SC-TEC can be passively cooled by the external environment, reducing the active cooling energy consumption and thereby enhancing the overall system performance.

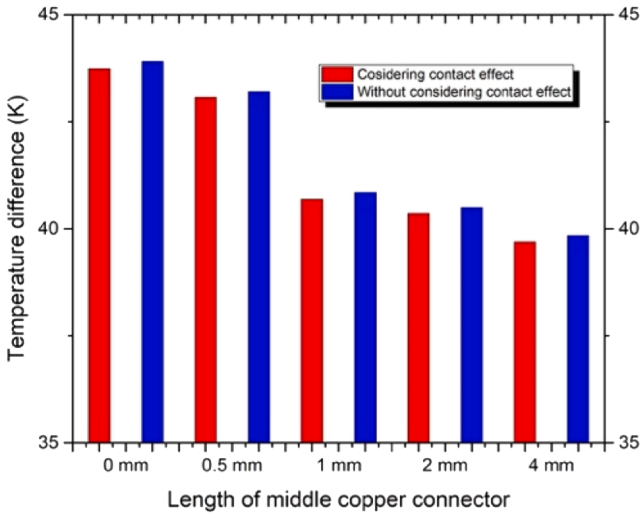

Fig. 7. Temperature difference of 5 normal size TECs with separated configuration with/without considering contact effect when input current of 5.5 A.

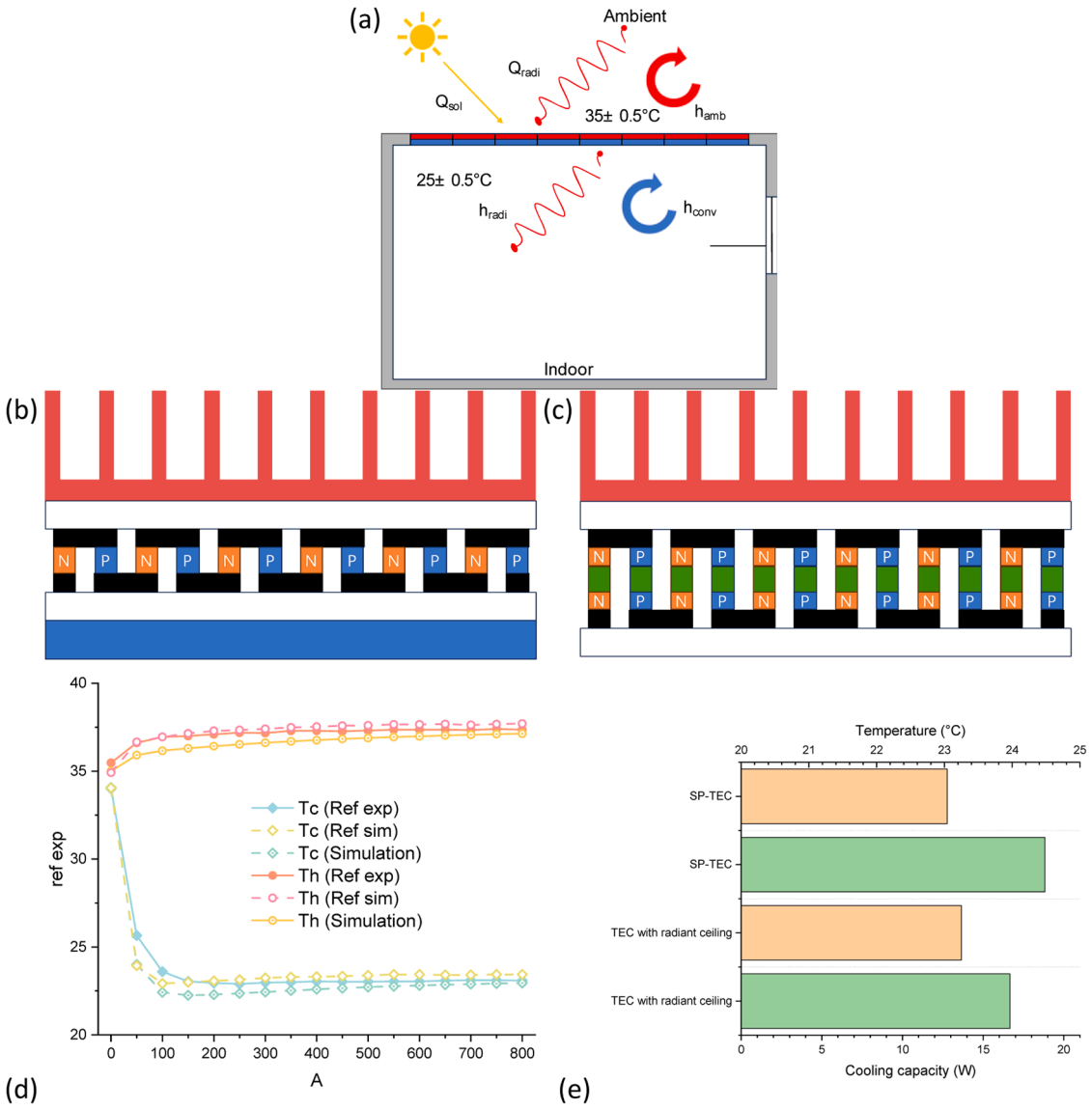

Fig. 8. Schematic, configuration, and performance for TEC/SC-TEC building ceiling applications (a) Schematic diagram for testing system; (b) conventional TEC ceiling; (c) SC-TEC ceiling; (d) model validation via transient results with reference data; (e) TEC ceiling and SC-TEC ceiling performance comparison.

Furthermore, by utilizing a state of art material characterized by low thermal and electrical resistance, the adverse impact from the middle metal strips could be removed, enabling the SC-TEC to achieve flawless performance without any losses. This supports the reliability of the SC-TEC. Moreover, the SC-TEC enables the device design flexibly, thus paving a path towards building integrated thermoelectric air conditioning.

3.4. *Impact of contact effect on traditional and separated-configuration structure TEC in normal size*

To further validate the impact of contact effect on normal-sized TECs, simulations were conducted for the five devices mentioned above, with an input current of 5.5 A. This analysis considered both scenarios: with and without contact effects on the hot-cold surface temperature difference. The results are depicted in Fig. 7.

As depicted in Fig. 7, the temperature variation caused by contact effects is relatively minimal, accounting for only 0.16 %. Unlike micro-TECs, the influence of contact effects on the performance of regular-sized TECs is negligible. This is attributed to the fact that in normal-sized TECs, the Seebeck cooling, and Joule heating effects are significantly more pronounced than the heat generated by contact effects.

3.5. *Case study of the SC-TEC in an application scenario*

After analysing and investigating the performance refer to the SC-TEC, which illustrates the feasibility of the novel design, we will further explore the SC-TEC in a practical application scenario, and discuss the structure, their performance, and the system superiority.

A practical experiment was carried out in an enthalpy difference laboratory refer to Ref [30]. The test involved two chambers in the laboratory, each set at different temperatures to simulate the indoor and outdoor environments. The SC-TEC was positioned at the opening between the two chambers, with its cold surface exposed to the cooling chamber (25± 0.5°C) and hot surface exposed to the heating chamber (about 35± 0.5°C).

The test system is shown schematically in Fig. 8a. It included 4 TE modules of TEC1-13910, which are interconnected electrically in series and thermally in parallel, an aluminum plate-fin heat sink, which is affixed to the hot surface to dissipate heat to the surrounding environment, two axial flow fans, which are utilized to enhance heat dissipation

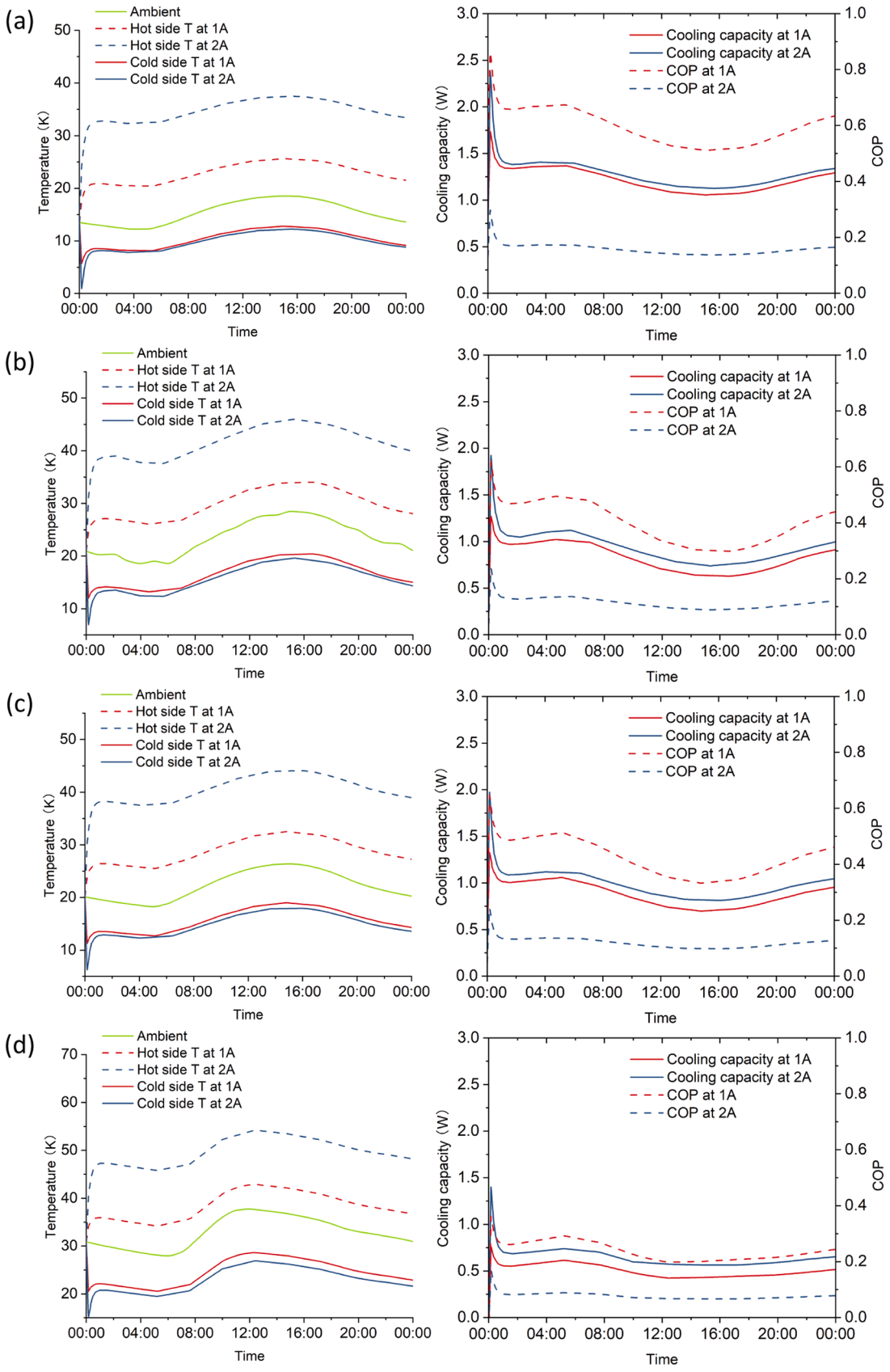

Fig. 9. SC-TEC system's performance under passive cooling at (a) London; (b) Beijing; (c) Washington; (d) Dubai.

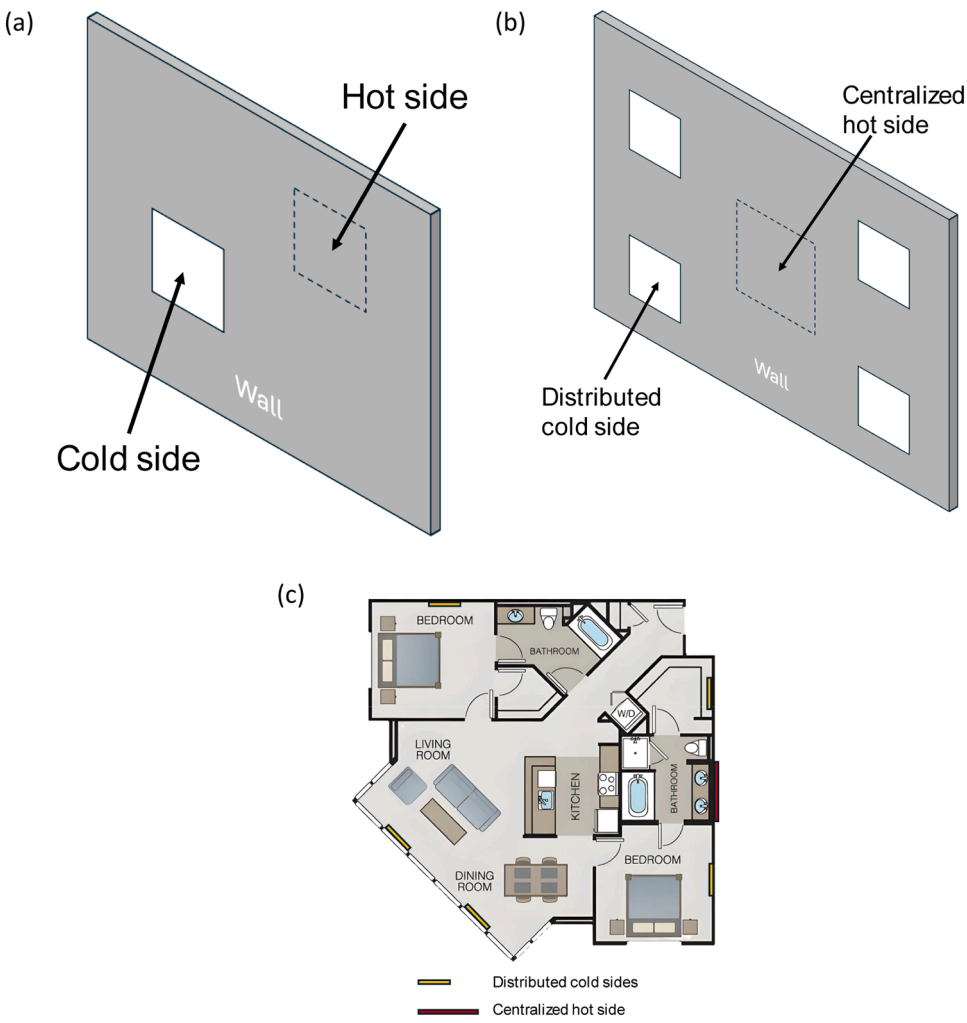

Fig. 10. Blueprint of (a) Blueprint of staggered or offset cold/hot side positioning TEC; (b) centralized hot side to distributed cold side TEC; (c) Utilization scenario of separately-configured TEC.

at the hot surface, and a radiant ceiling (as shown in Fig. 8b), which enhance the heat absorption at the cold surface. For the SC-TEC system, the radiant ceiling is replaced by copper strips of equal height (as shown in Fig. 8c).

Fig. 8d illustrates the comparison between the test, simulation and reference results under the condition of 1.0 A over time. The simulation results demonstrate a strong agreement with the simulated and experimental results reported in the literature, the maximum error between the simulated results within 1°C, thus validating the simulation model employed in this study.

The cooling capacity and cold surface temperature for TEC-building system under steady state conditions are as shown in Fig. 8e. By introducing the SC-TEC, the cooling capacity of the TEC system increased from 16.66 W/m^2 to 18.82 W/m^2 by 13 %, while the cooling surface temperature is decreased by 0.2°C. The decrease in the cooling surface temperature increases the temperature difference between the cooled surface and the surrounding indoor environment. This larger temperature gradient enhances heat transfer to the environment, thereby increasing the cooling capacity. In fact, when the TEC is integrated with radiant ceiling to fit with the building envelope structure, its performance will be compromised.

To further analyze the practical performance of the SC-TEC ceiling system, a full-day simulation was conducted using climate data for a typical day in July. The selected locations include London, UK; Beijing, China; Washington, D.C., USA; and Dubai, UAE, representing typical climatic conditions from polar, temperate, and tropical regions, based on data from the American Society of Heating. The hot side of the SC-TEC system operates at the outdoor ambient temperature, while the cold side is maintained indoors, both utilizing passive heat exchange. The system performance for each location is as follows.

As shown in Fig. 9, the SC-TEC system demonstrates relatively better performance in low-temperature regions, such as London, with a cooling power of up to 1.5 W and a COP of 0.6. However, as regional temperatures increase, system performance gradually decreases. In high-temperature regions like Dubai, the cooling power drops to only 0.61 W, and the COP reduces to 0.28.

This performance variation is primarily due to the impact of the hot side temperature on the SC-TEC device. The results presented are based on natural heat exchange condition, in practical applications of TEC/SC-TEC systems, the hot side is often emploied active cooling. Under such conditions, the SC-TEC degisn's passive cooling capability, leveraging the outdoor environment, can assist active cooling methods, thereby reducing cooling energy consumption and enhancing the overall system performance.

4. Further design for the SC-TEC

When the losses of the additional heat transfer layer, which help embed the TEC within the building envelope structure, the results shows that the SC-TEC made from present materials could achieve a cooling

capacity increase by around 2 .16W. Additionally, the innovative structural design of the SC-TEC opens up the new possibilities.

Further development of this idea would allow: (a) The cold and hot side of the system to be staggered or offset from each other (Fig. 10a); the one hot side of the TEC to be coupled with multiple cold sides of the TEC, thus creating multiple-areas air conditioning with one centralized hot side by using SC-TEC module (Fig. 10b). Furthermore, the flexibility of the middle metal strip allows it to be embedded within walls, enabling centralized placement of the hot side while distributing the cold sides across multiple rooms. Thus, allows the hot side of the TEC to be positioned in a cool, ventilated space outside the building, significantly enhancing the energy efficiency of multi-room air conditioning operations. (Fig. 10c).

5. Conclusions

A model was developed to analyse the performance of a novel separately-configured thermoelectric cooler (SC-TEC) module. This model was firstly validated by experiment and case study from the former literature. The performance analysis of the device includes cooling capacity, coefficient of performance (COP) and a new case study were undertaken.

With current TEC materials, separated configuration led to 5.6 % reduction in cooling capacity, varying from 7.13 W to 6 .76W. The coefficient of performance (COP) achieved 4.4 and 1.9 separately under the temperature difference of 5 K and 10K. At present, the additional Joule heating and contact thermal resistance limit the performance of SC-TEC, with Joule heating being the primary factor affecting its performance.

It is anticipated that the development of new materials with low thermal and electrical resistance can create the potential to eliminate this performance degradation in the SC-TEC. By utilizing such advanced materials, it may be possible to achieve lossless performance and further enhance the efficiency and effectiveness of SC-TEC systems.

In practical applications, the SC-TEC system eliminates the need for a traditional radiant ceiling, leading to an increase in cooling capacity from 16.66 W/m^2 to 18.82 W/m^2, representing a 13 % performance improvement. The performance results of the SC-TEC system under passive cooling conditions in different regions indicate that its performance is constrained by the hot side temperature. However, the innovative structural design of the SC-TEC allows the outdoor environment to serve as auxiliary cooling for the TEC's hot side, reducing the energy consumption of active cooling and further improving overall performance. Furthermore, the application of this new structure breaks the limitations of the traditional TEC structure, suggesting that the SC-TEC has potential to open up new research direction in the building-TEC sector.

CRediT authorship contribution statement

Haowen Liu: Writing – original draft, Validation, Software, Methodology, Investigation, Formal analysis, Data curation, Conceptualization. **Limei Shen:** Writing – review & editing. **Yunhai Li:** Writing – review & editing, Data curation. **Xudong Zhao:** Supervision, Methodology, Funding acquisition, Conceptualization. **Guiqiang Li:** Supervision, Methodology, Formal analysis. **Zeyu Liu:** Data curation. **Hongxing Yang:** Writing – review & editing.

Declaration of competing interest

The authors declare that they have no known competing financial interests or personal relationships that could have appeared to influence the work reported in this paper.

Acknowledgements

Funding: This work is primarily supported by University of Hull – CSC funding. This work was performed in part at Huazhong University of Science and Technology.

Supplementary materials

Supplementary material associated with this article can be found, in the online version, at doi:10.1016/j.adapen.2025.100218.

Data availability

Data will be made available on request.

References

[1] "Buildings – Topics - IEA." Accessed: May 17, 2023. [Online]. Available: https://www.iea.org/topics/buildings.
[2] Buildings and construction sector – Huge untapped potential for emission reductions. 2023. Accessed: May 17[Online]. Available, https://www.unep.org/news-and-stories/press-release/buildings-and-construction-sector-huge-untapped-potential-emission.
[3] S.K. Alghoul and S.K.A. Alghoul, "A comparative study of energy consumption for residential HVAC systems using EnergyPlus," http://www.sciencepublishinggroup.com, vol. 2, no. 2, p. 98, 2017, doi: 10.11648/J.AJMIE.20170202.16.
[4] Qin Y, Qin B, Wang D, Chang C, Zhao LD. Solid-state cooling: thermoelectrics. Energy Environ Sci 2022;15(11):4527–41. https://doi.org/10.1039/D2EE02408J.
[5] Gillott M, Jiang L, Riffat S. An investigation of thermoelectric cooling devices for small-scale space conditioning applications in buildings. Int J Energy Res 2010;34(9):776–86. https://doi.org/10.1002/er.1591.
[6] S. Maneewan, W. Tipsaenprom, and C. Lertsatitthanakorn, "Thermal comfort study of a compact thermoelectric air conditioner", doi: 10.1007/s11664-010-1239-8.
[7] Irshad K, Habib K, Thirumalaiswamy N, Saha BB. Performance analysis of a thermoelectric air duct system for energy-efficient buildings. Energy 2015;91:1009–17. https://doi.org/10.1016/J.ENERGY.2015.08.102.
[8] Irshad K, Habib K, Basrawi F, Saha B. Study of a thermoelectric air duct system assisted by photovoltaic wall for space cooling in tropical climate. 2016. https://doi.org/10.1016/j.energy.2016.10.110.
[9] Irshad K, Habib K, Basrawi F, Thirumalaiswamy N, Saidur R, Saha BB. Thermal comfort study of a building equipped with thermoelectric air duct system for tropical climate. Appl Therm Eng 2015;91:1141–55. https://doi.org/10.1016/J.APPLTHERMALENG.2015.08.077.
[10] Irshad K, Habib K, Algarni S, Saha BB, Jamil B. Sizing and life-cycle assessment of building integrated thermoelectric air cooling and photovoltaic wall system. Appl Therm Eng May 2019;154:302–14. https://doi.org/10.1016/J.APPLTHERMALENG.2019.03.027.
[11] Allouhi A, et al. Dynamic analysis of a thermoelectric heating system for space heating in a continuous-occupancy office room. Appl Therm Eng 2017;113:150–9. https://doi.org/10.1016/J.APPLTHERMALENG.2016.11.001.
[12] Kim YW, Ramousse J, Fraisse G, Dalicieux P, Baranek P. Optimal sizing of a thermoelectric heat pump (THP) for heating energy-efficient buildings. Energy Build 2014;70:106–16. https://doi.org/10.1016/j.enbuild.2013.11.021.
[13] Cai Y, Zhang DD, Liu D, Zhao FY, Wang HQ. Air source thermoelectric heat pump for simultaneous cold air delivery and hot water supply: full modeling and performance evaluation. Renew Energy 2019;130:968–81. https://doi.org/10.1016/j.renene.2018.07.007.
[14] Cai Y, Mei SJ, Liu D, Zhao FY, Wang HQ. Thermoelectric heat recovery units applied in the energy harvest built ventilation: parametric investigation and performance optimization. Energy Convers Manag 2018;171(January):1163–76. https://doi.org/10.1016/j.enconman.2018.06.058.
[15] Tipsaenporm W, et al. Improvement of cooling performance of a compact thermoelectric air conditioner using a direct evaporative cooling system. JEMat 2012;41(6):1186–92. https://doi.org/10.1007/S11664-012-1909-9.
[16] Cai Y, Wang L, Ding WT, Liu D, Zhao FY. Thermal performance of an active thermoelectric ventilation system applied for built space cooling: network model and finite time thermodynamic optimization. Energy 2019;170:915–30. https://doi.org/10.1016/j.energy.2018.12.186.
[17] Bergman T, Bergman T, Incropera F, Dewitt D. Fundamentals of heat and mass transfer. 2011.
[18] Shoeibi S, Kargarsharifabad H, Khiadani M, Parsa SM, Mirjalily SAA, Mohammed HA. Techniques used to enhance condensation rate of solar desalination systems: state-of-the-art review. Int Commun Heat Mass Transf 2024;159:108164. https://doi.org/10.1016/J.ICHEATMASSTRANSFER.2024.108164.
[19] Qamar A, et al. Advancing sustainable cooling: performance analysis of a solar-driven thermoelectric refrigeration system for eco-friendly solutions. Case Stud Therm Eng 2024;60:104781. https://doi.org/10.1016/J.CSITE.2024.104781.
[20] Faheem M, Abu Bakr M, Ali M, Majeed MA, Haider ZM, Khan MO. Evaluation of efficiency enhancement in photovoltaic panels via integrated thermoelectric cooling and power generation. Energies 2024 May 2024;17(11):2590. https://doi.org/10.3390/EN17112590.

[21] Ahmed HA, Megahed TF, Nada S, Mori S, Hassan H. Impact of modules number of thermoelectric cooler coupled with PV panels and phase change material on building air conditioning. J Build Eng 2024;86:108914. https://doi.org/10.1016/J.JOBE.2024.108914.
[22] Chandel R, Chandel SS, Prasad D, Dwivedi RP. Experimental analysis and modelling of a photovoltaic powered thermoelectric solid-state cooling system for transition towards net zero energy buildings under different solar loading conditions. J Clean Prod 2024;442:141099. https://doi.org/10.1016/J.JCLEPRO.2024.141099.
[23] Wang Y, Shukla A, Liu S. A state of art review on methodologies for heat transfer and energy flow characteristics of the active building envelopes. Renew Sustain Energy Rev 2017;78:1102–16. https://doi.org/10.1016/J.RSER.2017.05.015.
[24] Liu Z, Zhang L, Gong G, Luo Y, Meng F. Evaluation of a prototype active solar thermoelectric radiant wall system in winter conditions. Appl Therm Eng 2015;89:36–43. https://doi.org/10.1016/j.applthermaleng.2015.05.076.
[25] Prieto A, Knaack U, Auer T, Klein T. Solar coolfacades: framework for the integration of solar cooling technologies in the building envelope. Energy 2017;137:353–68. https://doi.org/10.1016/J.ENERGY.2017.04.141.
[26] Ibáñez-Puy M, Joś J, Antonio J, Fernández S, ‘ Esar Martín-G ‘ Omez C, Vidaurre-Arbizu M. Development and construction of a thermoelectric active facade module. J Facade Des Eng 2015;3(1):15–25. https://doi.org/10.3233/FDE-150025.
[27] Liu ZB, Zhang L, Gong GC, Luo YQ, Meng FF. Experimental study and performance analysis of a solar thermoelectric air conditioner with hot water supply. Energy Build 2015;86:619–25. https://doi.org/10.1016/J.ENBUILD.2014.10.053.
[28] Roohi R, Amiri MJ, Akbari M. Implementation of thermoelectric wall systems for sustainable indoor environment regulation in buildings through numerical and experimental performance analysis. Scientif Rep 2024 2024;14(1):1–18. https://doi.org/10.1038/s41598-024-78419-x. 14, no. 1.
[29] Arias-Salazar P, Zuazua-Ros A, Sacristán-Fernández JA, He Z, Vidaurre-Arbizu M, Martín-Gómez C. Thermoelectric active window frame: constructive integration and preheating analysis. J Build Eng 2024;94:109888. https://doi.org/10.1016/J.JOBE.2024.109888.
[30] Su X, Zhang L, Liu Z, Luo Y, Chen D, Li W. Performance evaluation of a novel building envelope integrated with thermoelectric cooler and radiative sky cooler. Renew Energy 2021;171:1061–78. https://doi.org/10.1016/j.renene.2021.02.164.
[31] Luo Y, Zhang L, Liu Z, Wang Y, Meng F, Xie L. Modeling of the surface temperature field of a thermoelectric radiant ceiling panel system. Appl Energy 2016;162:675–86. https://doi.org/10.1016/J.APENERGY.2015.10.139.
[32] Shen L, Xiao F, Chen H, Wang S. Investigation of a novel thermoelectric radiant air-conditioning system. Energy Build 2013;59:123–32. https://doi.org/10.1016/J.ENBUILD.2012.12.041.
[33] Liu Z, Zhang L, Gong G. Experimental evaluation of a solar thermoelectric cooled ceiling combined with displacement ventilation system. Energy Convers Manag 2014;87:559–65. https://doi.org/10.1016/J.ENCONMAN.2014.07.051.
[34] Ibañez-Puy M, Bermejo-Busto J, Martín-Gómez C, Vidaurre-Arbizu M, Sacristán-Fernández JA. Thermoelectric cooling heating unit performance under real conditions. Appl Energy 2017;200:303–14. https://doi.org/10.1016/J.APENERGY.2017.05.020.
[35] Sun X, Ling L, Liao S, Chu Y, Fan S, Mo Y. A thermoelectric cooler coupled with a gravity-assisted heat pipe: an analysis from heat pipe perspective. Energy Convers Manag 2018;155:230–42. https://doi.org/10.1016/J.ENCONMAN.2017.10.068.
[36] He W, Zhou J, Hou J, Chen C, Ji J. Theoretical and experimental investigation on a thermoelectric cooling and heating system driven by solar. Appl Energy 2013;107:89–97. https://doi.org/10.1016/J.APENERGY.2013.01.055.
[37] Riffat SB, Ma X, Wilson R. Performance simulation and experimental testing of a novel thermoelectric heat pump system. Appl Therm Eng 2006;26(5–6):494–501. https://doi.org/10.1016/J.APPLTHERMALENG.2005.07.016.
[38] Luo Y, Zhang L, Liu Z, Wang Y, Meng F, Wu J. Thermal performance evaluation of an active building integrated photovoltaic thermoelectric wall system. Appl Energy 2016;177:25–39. https://doi.org/10.1016/J.APENERGY.2016.05.087.
[39] Wang C, Calderón C, Wang YD. An experimental study of a thermoelectric heat exchange module for domestic space heating. Energy Build 2017;145:1–21. https://doi.org/10.1016/J.ENBUILD.2017.03.050.
[40] Cosnier M, Fraisse G, Luo L. An experimental and numerical study of a thermoelectric air-cooling and air-heating system. Int J Refrigerat 2008;31(6):1051–62. https://doi.org/10.1016/J.IJREFRIG.2007.12.009.
[41] He W, Zhou J, Hou J, Chen C, Ji J. Theoretical and experimental investigation on a thermoelectric cooling and heating system driven by solar. Appl Energy 2013;107:89–97. https://doi.org/10.1016/J.APENERGY.2013.01.055.
[42] Riffat SB, Ma X, Wilson R. Performance simulation and experimental testing of a novel thermoelectric heat pump system. Appl Therm Eng 2006;26(5–6):494–501. https://doi.org/10.1016/J.APPLTHERMALENG.2005.07.016.
[43] He W, Zhou J, Chen C, Ji J. Experimental study and performance analysis of a thermoelectric cooling and heating system driven by a photovoltaic/thermal system in summer and winter operation modes. Energy Convers Manag 2014;84:41–9. https://doi.org/10.1016/J.ENCONMAN.2014.04.019.
[44] Zhang HY. A general approach in evaluating and optimizing thermoelectric coolers. Int J Refrigerat 2010;33(6):1187–96. https://doi.org/10.1016/J.IJREFRIG.2010.04.007.

Further reading

[45] Sun D, et al. Modeling and analysis of the influence of Thomson effect on micro-thermoelectric coolers considering interfacial and size effects. Energy 2020;196:117116. https://doi.org/10.1016/J.ENERGY.2020.117116.
[46] Liu H, Zhao X, Li G, Ma X. Investigation of a novel separately-configured micro-thermoelectric cooler to enabling extend application scope. Appl Energy 2022;306:117941. https://doi.org/10.1016/J.APENERGY.2021.117941.